Int J Adv Manuf Technol (2014) 70:1143–1155
DOI 10.1007/s00170-013-5334-x

ORIGINAL ARTICLE

Investigating the optimum molybdenum disulfide (MoS_2) nanolubrication parameters in CNC milling of AL6061-T6 alloy

Bizhan Rahmati · Ahmed A. D. Sarhan · M. Sayuti

Received: 25 July 2012 / Accepted: 23 September 2013 / Published online: 13 October 2013

Abstract Aluminum 6061-T6 is an important alloy as it has dominant mechanical properties like weldability and hardness, and has the potential to be used at variable temperatures. AL6061-T6 is frequently used in the aerospace industry, as well as aircraft, automotive, and packaging food industries. Milling of Al6061-T6 is important especially to produce various product shapes for adapting to diverse applications. The aptitude of the CNC milling machine for batch production would be a noteworthy advantage. However, the demand for high quality brings attention to product quality, particularly the roughness of the machined surface because of its effect on product appearance, function, and reliability. Introducing correct lubrication to the machining zone could improve the tribological characteristics of Al6061-T6. For additional improvement, applying nanolubrication may produce superior product quality, as the rolling action of billions of nanoparticle units in the tool chip interface can significantly decrease the cutting forces. In this research work, the optimum MoS_2 nanolubrication parameters in Al6061-T6 milling to achieve the lowest cutting force, cutting temperature and surface roughness are investigated. The parameters include nanolubricant concentration, nozzle orientation and air carrier pressure. Taguchi optimization along with standard orthogonal array $L_{16}(4^3)$ are employed. Furthermore, surface roughness and cutting force are analyzed via signal-to-noise (S/N) response analysis and the analysis of variance (Pareto ANOVA) in the hopes of achieving optimum conditions and to determine which process parameters are statistically significant. Finally, optimization improvements are investigated through confirmation tests.

Keywords MoS_2 nanolubrication · End milling · Surface roughness · Cutting force · Al6061-T6 alloy

B. Rahmati (✉) · A. A. D. Sarhan · M. Sayuti
Centre of Advanced Manufacturing and Material Processing, Department of Design and Manufacturing, Engineering Faculty, University of Malaya, 50603 Kuala Lumpur, Malaysia
e-mail: r.bijan@yahoo.com

B. Rahmati
Department of Mechanical Engineering, Engineering Faculty, Tehran University, Tehran, Iran

A. A. D. Sarhan
Department of Mechanical Engineering, Faculty of Engineering, Assiut University, Assiut 71516, Egypt

1 Introduction

Aluminum has advantages above other materials comprising a high strength/weight ratio, corrosion resistance and formability. Alloys 6061, 7075, and 2024, sometimes referred to "aerospace alloys" due to their partial applications in the aeronautics industry. These alloys are engineered to be lightweight and strong. Their ease of formability allows complex shapes and parts to be drawn, which can then be further enhanced with heat treatment. Aluminum AL6061-T6 is an alloy which contains magnesium and silicon as major alloying elements, and commonly serves several purposes due to the superior mechanical properties such as hardness and good weldability [1, 2] as well as the solutionized and tempered-grade characteristic of this type of aluminum. Widespread applications for this type of material are found in the aircraft, automotive, and food packaging industries. The capability of the CNC milling machine to produce intricate, special products may be a noteworthy advantage for aluminum AL6061-T6. However, the demand for high quality brings attention to a product's quality and surface condition, especially machined surface roughness — because of its effect on product appearance, function, and reliability [3, 4].

The tribological characteristics of the machining process can be improved by introducing lubrication into the

machining regions [5, 6]. Applying lubrication correctly reduces friction at the tool–chip interface, resulting in enhanced surface quality. Despite the significance of lubrication in machining being widely recognized, conventional flooding application in machining processes has become a huge liability. Such fluids are difficult to dispose of, expensive to recycle and can cause skin and lung diseases to operators. The increasingly stricter environmental regulations and enforcement are also eliminating much of the flexibility with using cutting fluids [7, 8]. Moreover, from an economical perspective, the costs associated with the usage of lubricants is estimated to be several billion US$ yearly. The cost related to lubrication and cutting fluid is 17 % of the total production cost, which is normally higher than that of cutting tool equipment which incurs only 7.5 % of the total cost. Consequently, eliminating lubricants if possible may be a significant economic incentive [9, 10].

Lubrication research is deemed to increase in response to a demand for it. In the past, demand arose when new technologies posed new challenges, e.g.,*** space stations, adiabatic diesel engines, and ultra-high storage density in magnetic hard disks. Such new technologies pose a burden outside the existing knowledge base, such as high temperatures, radiation, and nanometer scale precision [4]. At present, countless efforts are being made to develop advanced machining processes using less lubrication [11]. A promising alternative to conventional flood coolant applications is minimum quantity lubrication (MQL). Klocke and Eisenblätter [12] stated that MQL refers to only a minute amount of lubrication used — typically, a flow rate of 50 to 500 ml/h, or about 3 to 4 orders of magnitude lower than the amount normally used in flood cooling conditions. This has been reported to reduce friction, cutting temperature and improve tool life due to the lubricant's ability to penetrate into the chip–tool interface, thus improving the product's surface quality. However, the respective surface quality improvement is a function of the MQL lubrication parameters that include air pressure and nozzle angle (better known as lubrication factors system). The MQL system is adjusted according to these parameters to deliver lubricant. For further improvement, introducing nanolubrication could produce much better product quality as the rolling action of billions of units of nanoparticles in the tool–chip interface could notably reduce cutting forces. The structure, shape and size of nanoparticles play an important role in their tribological properties [13, 14]; however, nanoparticle concentration in oil is an essential parameter for investigation to determine the optimum surface quality.

Up to now, several nanolubricants have been identified by advancements in modern technology — nanolubricants which can sustain and provide lubricity over a wide range of temperatures [15, 16]. The effectiveness of lubrication is dependent on quantity, the morphology and crystal structure of solid lubricants, and the way that particles get introduced to the tool–workpiece interface [17]. Nanolubricants comprise a kind of new engineering material consisting of nanometer-sized particles distributed in base oil. It is potentially an effective method to reduce friction between two contact surfaces, depending on the working conditions. Lubricants are expected to withstand the high machining temperatures, and be non-toxic, easy to apply and cost-effective [18]. On the other hand, physical analysis of nanolubricants [19] demonstrates that dispersed nanoparticles can easily penetrate into the rubbing surfaces and have a large elastohydrodynamic lubrication effect. According to researchers, under a single-thrust bearing tester the nanolubricant's coefficient of friction is less than that of pure oil while the extreme pressure of the nanolubricant is two times higher than that of pure oil; hence it can be deduced that the nanolubricant improves lubrication performance by averting contact between the metal surfaces. Moreover, the thermal conductivity of a nanolubricant increases linearly with the concentration, thus facilitating hydrodynamic interaction to enhance thermal transport capability [20–23].

Molybdenum disulfide (MoS_2) nanoparticles make a hard, brittle material that is cheap and readily available on the market. MoS_2 possesses excellent mechanical properties especially in terms of hardness. Size ranges from 20 to 100 nm, and the ideal range to be used in machining applications is 20 to 60 nm, as it could be easily and effectively accelerated by an MQL system into the machining zone [21].

In this study the authors are investigating the optimum molybdenum disulfide (MoS_2) nanolubrication parameters in CNC milling of AL6061-T6 alloy to achieve the best surface quality, lowest cutting force and lowest cutting temperature. These parameters include nanolubricant concentration, nozzle orientation and pressurized air (hereafter called control factors). The conventional technique to optimize this process is the "trial and error" approach, yet it is very time consuming due to the requirement of a large number of experiments. Hence, a reliable systematic approach for optimizing machining parameters is necessary. Taguchi optimization is an efficient, effective, reliable and simpler approach, in which the response parameters affecting surface roughness, cutting forces and cutting temperature can be optimized [24]. The stages in the Taguchi optimization method include: selecting the orthogonal array (OA) according to the numbers of controllable factors, running experiments based on the OA, analyzing data, identifying the optimum parameters, and conducting confirmation runs with the most favorable levels of all parameters.

2 Experimental design

The standardized Taguchi method was employed according to the experimental design of an $L_{16}(4^3)$ OA in order to achieve

Table 1 Control factors and experimental condition levels

Symbol	Variable factors	Level			
		$i=1$	$i=2$	$i=3$	$i=4$
A	Nanoparticle concentration (wt%)	0 %	0.20 %	0.50 %	1 %
B	Air pressure (bar)	1	2	3	4
C	Nozzle orientation (Deg)	15°	30°	45°	60°

the lowest cutting force, cutting temperature and surface roughness. The standard OA consists of 16 tests with three control factors and four different experimental state levels for each factor. The stated factors and levels are specified in Table 1. The 16 experiments and the details of the combinations of experimental condition levels for each control factor (A–C) are shown in Table 2. All experiments were carried out in a random sequence to remove any other invisible factors that may also affect cutting force, cutting temperature and surface roughness.

Following OA selection, the Taguchi optimization method entails running the experiments based on the chosen OA. The experimental setup is shown in Fig. 1. The machine used is a vertical type machining center (Mitsui Seiki VT3A). The spindle has constant position preload bearings with oil–air lubrication, while the maximum rotational speed and power are 20,000 min^{-1} and 15 kW, respectively. To investigate the cutting forces, a slot-milling test was carried out in the cutting process of a $40\times40\times100$ mm^3 rectangular aluminum AL6061-T6 workpiece and using the proposed experimental setup. The mechanical properties of aluminum AL6061-T6 are shown in Table 3 [25].

Table 2 Standard L_{16} $(4)^3$ orthogonal array

Experiment no.	Control factors and levels (i)		
	A	B	C
1	$i=1$	1	1
2	$i=1$	2	2
3	$i=1$	3	3
4	$i=1$	4	4
5	$i=2$	1	2
6	$i=2$	2	1
7	$i=2$	3	4
8	$i=2$	4	3
9	$i=3$	1	3
10	$i=3$	2	4
11	$i=3$	3	1
12	$i=3$	4	2
13	$i=4$	1	4
14	$i=4$	2	3
15	$i=4$	3	2
16	$i=4$	4	1

The 16 experiments with details of the combination levels

The cutting tool is tungsten carbide (AE302100) with two flutes and 10 mm in diameter, and is suitable for aluminum alloy milling. The tool moves in $+X$ direction to cut a stroke of 100 mm. Figure 2 illustrates the workpiece and its tool paths. The cutting speed, feed and depth of cut employed are 8,000 min^{-1}, 2,100 mm/min and 5 mm, respectively, as selected based on the tool manufacturer's recommendations. Cutting forces were measured with a Kistler three-axis dynamometer (type 9255B). The measured cutting force signals (X, Y, and Z directions) were captured and filtered through low-path filters (10-Hz cutoff frequency), while the cutting temperature was measured with a thermocouple (OAKTON, Temp JKT-Acron SeriesType TWD-35627-00, -02); each test measurement was repeated three times. The thermocouple was installed under the machining surface as per Fig. 1 and the specifications in Table 4. The measured temperature reflects the amount of heat dissipated in the workpiece. This amount of heat should indicate the change in the coefficient of friction between tool and chip in the cutting zone. For every machining run, the temperature was measured during the cutting process and surface roughness was measured using a surface profilometer (Mitutoyo SJ-201). Every experiment was repeated three times and surface roughness was measured at three regions for each cutting. Subsequently, the average of the data was calculated (Table 6). This table includes measured surface roughness under a variety of parameter combinations. Different surfaces were generated when different nanoparticle concentrations were combined with other parameters.

The two types of lubrication employed in this investigation are ordinary lubricant oil and Nanolubricant. The ECOCUT HSG 905S neat cutting oil from FUCHS was applied in both lubrication modes as base oil. This oil is free from phenol, chlorine or other additives. Preparation consisted of adding MoS_2 nanoparticles with an average size of 20–60 nm to the mineral oil for 48 h in order to suspend the particles homogeneously in the mixture. The mechanical properties of MoS_2 are presented in Table 5.

Oil was delivered to the tool–chip interface region via MQL. In the experiment, a thin-pulsed jet nozzle developed in the laboratory and controlled by a variable pressure and speed control drive was used. In case of the MoS_2

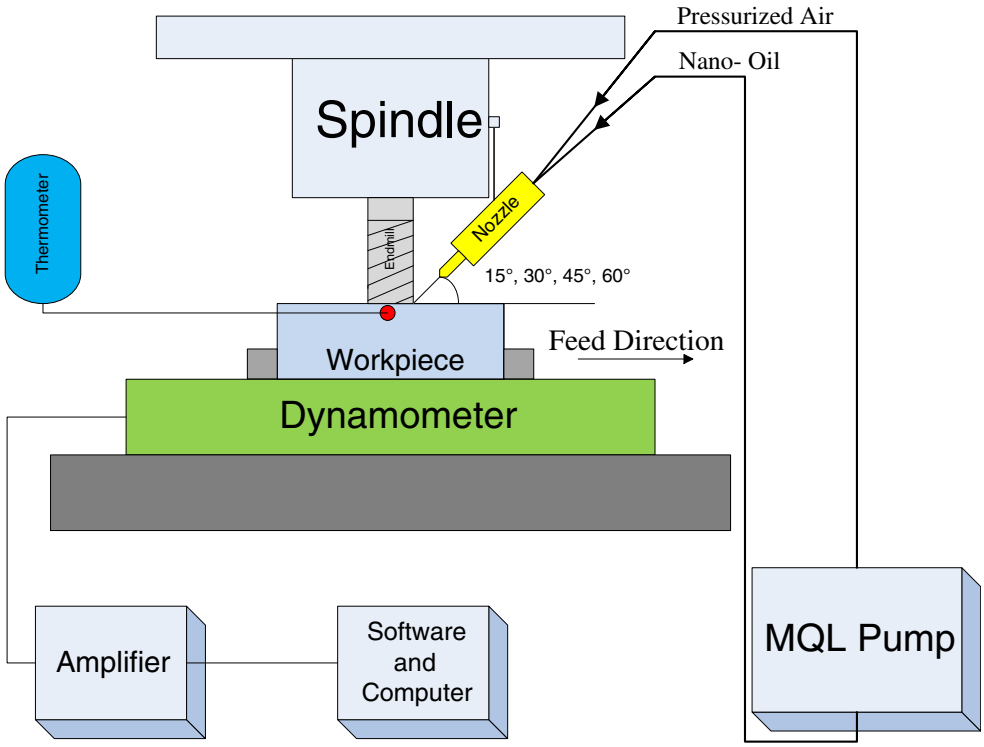

Fig. 1 Experimental set-up

nanolubrication system, the nozzle was equipped with an additional air nozzle to accelerate the lubricant into the cutting region and to decrease the amount of oil fed up to 25 %. The nozzle system was installed to a flexible and portable junction connected to the machining spindle. The nozzle can be set in any favorable direction because if it is equipped to a flexible connection then it does not interfere with the tool or workpiece during machining. The nozzle orifice diameter is 1 mm and the MQL oil pressure was set to 20 MPa with a delivery rate of 30 ml/min. Figure 3 presents the nozzle schematic sketch.

3 Experimental results, analysis and discussion

3.1 Experimental results

The cutting–milling test was done with the aim of investigating machining performance in line with the suggested experimental setup. Table 6 displays the measured values of cutting force, cutting temperature and surface roughness.

Table 3 Mechanical properties of aluminum (AL6061-T6) [25]

Ultimate tensile strength (MPa)		0.2 % Proof stress (MPa)		Webster hardness tester (model B)		Hardness Vickers (HV)
Min	Typical	Min	Typical	Min	Typical	Typical
260	310	240	275	8′	15′	105

3.2 Data analysis

Data analysis entails parameter optimization, identifying which process parameters are statistically significant, noise (signal-to-noise [S/N]) response analysis, interaction analysis and analysis of variance (Pareto ANOVA).

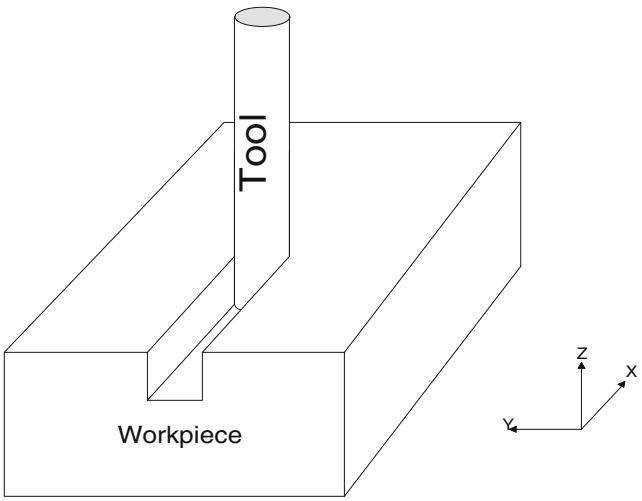

Fig. 2 The workpiece and tool paths

Table 4 OAKTON-type JKT thermocouple specification

Specification	Range
Measuring Range	−250 °C to 400 °C
Accuracy	±0.25 % of reading plus 1 °C/2 °F for temperatures <−99.9 °C/°F; ±0.2 % of reading plus 0.5 °C/0.9 °F for temperatures >−99.9 °C/°F
Resolution	0.1 °C (−99.9 °C to 299.9 °C) 1 °C (outside this range)

3.2.1 (S/N) response analysis

The methods for calculating S/N ratio are classified into three key classes, depending on whether the favorite quality characteristics are larger the better, smaller the better or nominal the better. In this case, for cutting force, cutting temperature and surface roughness, the smaller values are always favored. The equation for calculating the S/N ratio (in dB) is as follows:

$$\mathrm{S}\Big/\mathrm{N} = -10\log\frac{1}{n}\left(\sum y_i^2\right)_j, \quad (1)$$

where n is the number of individual measured responses (in this case, $n=3$), y_i is the individual measured cutting force, cutting temperature and surface roughness (Table 6) and j is the experiment number from 1 to 16. The S/N values function shown in Eq. 1 is a performance measurement parameter to develop processes insensitive to noise factors. For each factor, S/N ratios define the degree of predictable performance of a process in the presence of noise factors. Table 7 shows the calculated S/N ratio.

Figures 4, 5 and 6 illustrate the S/N response graphs for selecting the best combination levels for the lowest cutting forces, cutting temperature and surface roughness, respectively. The largest S/N response would reflect the best response which results in the lowest noise. This is the criteria employed in this study to determine the optimal parameters. From Fig. 4, it can be seen that nanoparticle concentration (A4, 1 wt.%) at air pressure (B4, 4 bars) and nozzle orientation (C2, 30°) is deemed an ideal choice for obtaining the lowest cutting force. Meanwhile, Fig. 5 indicates that nanoparticle concentration (A3, 0.5 wt.%) with air pressure (B4, 4 bars) and nozzle orientation (C2, 30°) is determined to be the best choice for obtaining the lowest cutting temperature. On the other hand, based on the S/N ratio criteria and Fig. 6, the nanoparticle concentration (A3, 0.5 wt.%) and air pressure (B4, 4 bars) with nozzle orientation (C4, 60°) is seemingly the best choice for achieving the lowest surface roughness. Basically, the optimal parameter combinations for lower cutting force, cutting temperature and surface roughness are (A4 B4 C2), (A3 B4 C2) and (A3 B4 C4), respectively.

Table 5 The mechanical properties of MoS_2

Properties	MoS2
Cristal structure	Hexagonal-layered
Melting point (°C)	1185
Density (g/cm^3)	4.8–5.0
Molecular weight (g/mol)	160.06
Color	Lead gray to black
Thermal conductivity at 300 K (W/cm °K)	0.014
Coefficient of friction	0.03–0.06
Hardness (Mohs scale) basal plane	1–1.5

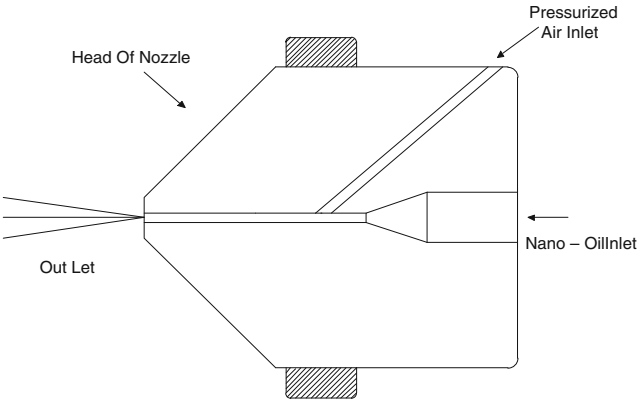

Fig. 3 Schematic drawing of the nozzle

3.2.2 Interaction analysis

To examine the data for the optimization process, interaction analysis served as an alternative analysis method. Cutting force, cutting temperature and surface roughness interaction data analysis is tabulated in Tables 8, 9 and 10, correspondingly, according to the S/N ratio data from Table 7. It was found that (A4 B4 C2), (A3 B4 C2) and (A3 B4 C4) are the optimal parameter combinations to get the lowest cutting force, cutting temperature and surface roughness values, respectively.

3.2.3 Analysis of variance (Pareto ANOVA): an alternative analysis

An alternative to analyzing data for the optimization process involves analysis of variance using Pareto ANOVA. The summation of squares of differences (S) for each control factor is calculated such that, for example, S_A can be obtained by the following equation:

$$S_A = (A_1-A_2)^2 + (A_1-A_3)^2 + (A_2-A_3)^2 + (A_3-A_4)^2 \quad (2)$$

S_B and S_C are calculated in the same manner. The contribution ratio for each factor is calculated as the percentage of

Table 6 The measured values of cutting force, cutting temperature and surface roughness (R_a)

Experiment no.	Measured values											
	Cutting force (N)				Cutting temperature (°C)				Surface roughness (μm)			
	Reading			Average	Reading			Average	Reading			Average
	1	2	3		1	2	3		1	2	3	
1	126.31	130.08	130.31	128.90	34.20	39.00	35.00	36.07	2.12	1.92	1.66	1.90
2	103.21	116.96	103.73	107.96	30.20	31.50	31.50	31.07	3.03	4.68	3.25	3.65
3	107.56	95.08	111.92	104.85	53.50	37.50	37.90	42.97	0.36	0.76	0.54	0.55
4	130.61	118.94	125.90	125.15	36.10	35.50	36.60	36.07	1.29	0.84	0.89	1.01
5	133.07	124.55	133.80	130.47	35.70	38.00	38.20	37.30	1.17	0.86	0.84	0.96
6	111.66	112.81	106.22	110.23	33.00	35.90	35.90	34.93	1.19	1.27	1.19	1.22
7	139.03	133.67	145.80	139.50	36.80	38.10	38.70	37.87	1.13	1.17	1.34	1.21
8	104.32	106.07	99.50	103.30	33.50	34.00	34.20	33.90	0.96	0.97	0.98	0.97
9	133.92	142.94	118.92	131.93	34.20	35.30	34.70	34.73	0.90	1.01	0.95	0.95
10	113.89	126.95	103.71	114.85	39.70	37.40	43.30	40.13	0.41	0.35	0.41	0.39
11	117.68	130.97	121.19	123.28	33.70	35.20	35.20	34.70	1.52	1.48	1.43	1.48
12	111.15	110.48	101.62	107.75	30.00	29.90	31.10	30.33	1.23	1.20	1.03	1.15
13	101.71	104.75	103.35	103.27	33.00	35.40	34.60	34.33	0.77	1.20	1.13	0.89
14	109.68	101.13	110.38	107.06	48.00	52.30	52.50	50.93	0.95	0.99	0.91	0.95
15	88.37	94.87	97.65	93.63	33.80	34.60	35.00	34.47	1.19	1.10	1.09	1.13
16	99.73	103.68	98.88	100.77	33.50	34.50	34.60	34.20	0.86	0.82	0.76	0.81

summation of squares of differences for each factor to the total summation of the squares of differences. The cumulative contribution and contribution ratio of all parameters for cutting force, cutting temperature and surface roughness are plotted in Figs. 7, 8 and 9.

Table 7 The calculated S/N ratio

Experiment no.	S/N ratio(dB)		
	Cutting force	Cutting temperature	Surface roughness
1	−42.21	−31.16	−5.61
2	−40.68	−29.85	−11.42
3	−40.43	−32.79	4.81
4	−41.95	−31.14	−0.24
5	−42.31	−31.44	0.28
6	−40.85	−30.87	−1.71
7	−42.90	−31.57	−1.70
8	−40.28	−30.60	0.26
9	−42.43	−30.82	0.39
10	−41.23	−32.09	8.15
11	−41.83	−30.81	−3.38
12	−40.66	−29.64	−1.26
13	−40.28	−30.72	0.82
14	−40.60	−34.15	0.45
15	−39.44	−30.75	−1.04
16	−40.07	−30.68	1.80

In Fig. 7, it is obvious that the best factor combination levels for minimum cutting force are: the nanoparticle concentration (A) with the highest contribution of 47.85 % followed by air pressure (B) with 35.55 % and finally, nozzle orientation (C) with 16.60 %. The air pressure and nanoparticle concentration are considered prominent factors, cumulatively contributing 83.40 %. Pareto ANOVA analysis suggests that A4 B4 C2 is the finest parameter combination to attain the least cutting force.

It is evident in Fig. 8 that nozzle orientation (C) contributions the most with 66.7 % followed by air pressure (B) with 22.66 % and nanoparticle concentration (A) with 10.63 %. Pareto ANOVA analysis recommends A3 B4 C2 as the finest parameter combination to obtain the lowest cutting temperature.

Lastly, Fig. 9 indicates that the best factor combination level for minimum surface roughness seems to be A3 B4 C4. The nanoparticle concentration and nozzle orientation parameters are considered prominent factors, having a cumulative contribution of 97.9 %.

In conclusion, the optimal parameter combinations for the lowest cutting force, cutting temperature and surface roughness achieved using Pareto ANOVA analysis are, respectively, (A4 B4 C2), (A3 B4 C2) and (A3 B4 C4), which are in

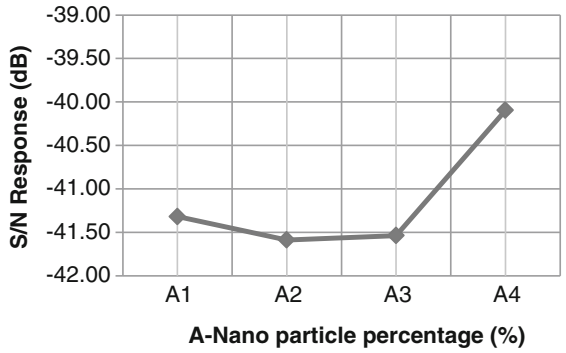

a) Nanoparticle concentration (A)

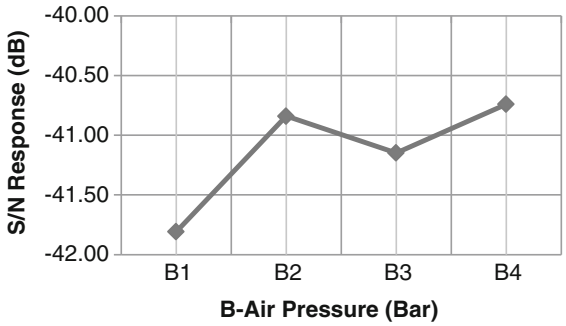

b) Air pressure (B)

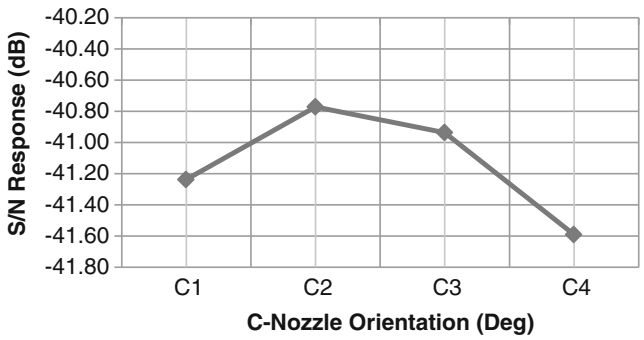

c) Nozzle orientation (C)

Fig. 4 S/N response graphs of cutting force at different parameter conditions

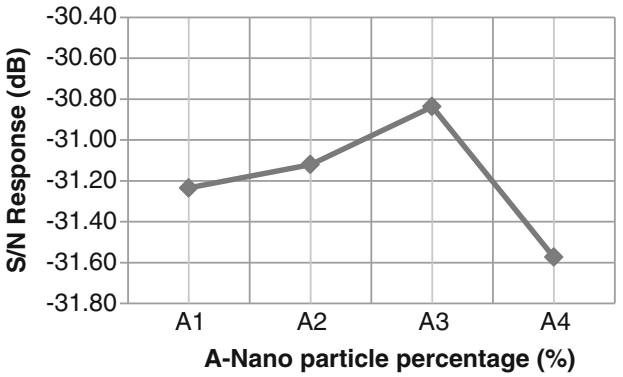

a) Nanoparticle concentration (A)

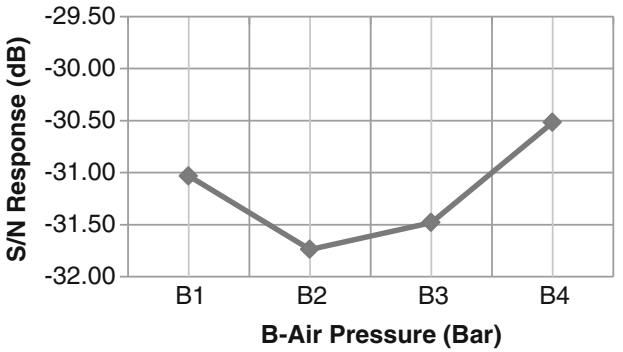

b) Air pressure (B)

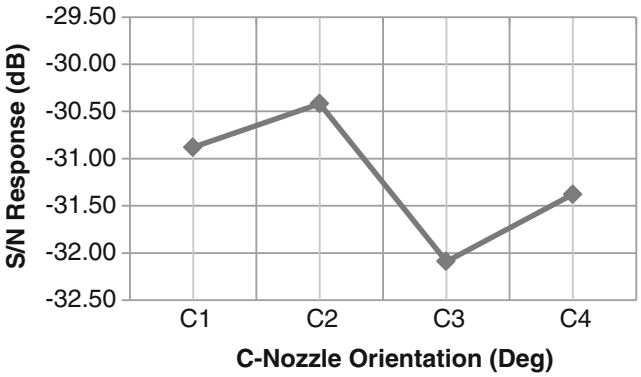

c) Nozzle orientation (C)

Fig. 5 S/N response graphs of cutting temperature at different parameter conditions

complete agreement with the results obtained previously using S/N and interaction response analysis.

4 Discussion

In the present study three data analysis techniques were used for investigation, and similar results were achieved among all methods. Spreading MoS_2 nanoparticles in cutting oil via pressurized air in the cutting region demonstrated respectable performance in decreasing subsequent cutting force, temperature and surface roughness. The gaps between the device surfaces are often filled only by nanometer particles. Present and future applications require high-speed relative motion, very light load, and numerous duty cycles. On a nanometer scale, the surface area to volume ratio for a typical component is very high, and surface forces become the dominant forces governing contact behavior [4]. The atomized spray form nano-oil exhibits more efficient feeding into the cutting zone than flood lubrication [26]. This may due to the splash of flood lubrication by the rotating cutting tool, while spray from the cutting oil may adhere on the tool workpiece interface and thus assist the cutting operation. The presence of helping nanoparticles in oil at the tool–workpiece interface have a

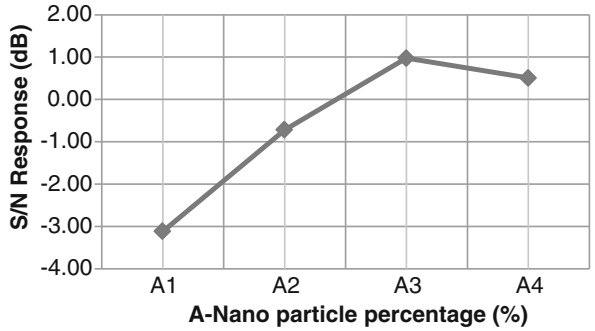

a) Nanoparticle concentration (A)

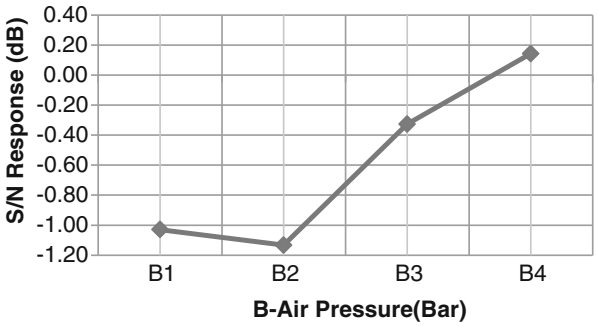

b) Air pressure (B)

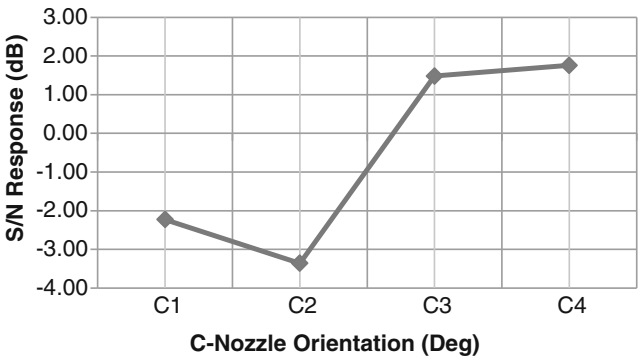

c) Nozzle orientation (C)

Fig. 6 S/N response graphs of surface roughness at different parameter conditions

burnish effect since an interacting force will then be induced at the interface between particles and tool surface [27]. This interacting force travels along the tool surface at a certain speed, after which it emits some power. Hung and Su [28] found that a large interacting force between particles and workpiece would reduce the surface energy of the workpiece — that is, the binding strength between the surface and sub-surface atoms of the workpiece. The breaking process requires a particular amount of energy to split the weakened work surface asperities and generate a new surface with lower roughness. The making process of nanoparticles transfers the potential energy from the tool, and then converts it into kinetic energy of surface atoms that dissipates as heat [28]. Consequently, more nanoparticles will be transferred at higher nano-oil concentrations, and therefore additional kinetic energy will shift to the workpiece surface and increase heat loss. Due to the low friction properties of nanoparticles, a significant impact on reducing the friction between tool and workpiece is observed alongside the consequent lowering of cutting forces.

Increasing nano-oil concentration raises the viscosity of cutting oil such that more nanoparticles will be present between tool and workpiece. This is one reason for eliminating the contact between the tool and workpiece. In high speed machining processes the abundant heat generated during cutting changes elastohydrodynamic lubrication into boundary lubrication; the spherical nanoparticles may create a rolling effect between the rubbing surfaces and reduce the coefficient of friction [29, 30]. The outcome of such cavities is thin caring film formation on the surfaces. In response to an increase of nano-oil concentration, the thin protecting film on the machined surface increases in thickness while larger number of nanoparticles will continue rubbing against the asperities at the workpiece surface during machining. More frequent exposure of the new surface to cutting oil results in strong chemical interaction to form between nano-oil and new surface. As a consequence, an extra intensive protective film is formed. The described process definitely increases machined surface quality while the coefficient of friction decreases [31].

The consumed energy transforms into heat at the deformation zones during the cutting process. The heat generated increases the cutting temperature alongside an increase of nano-oil concentration potentially reaching the work material's melting temperature. Another reason for the drastic increase of temperature may be the formation of thin film which refrains temperature from dispersing away from the machined surface. It could be supposed that temperature often raises the amount of material aiding grain boundary dislocation, hence easing the cutting operation, thus also lowering the cutting force [32, 33].

Throughout cutting, variations of pressurized stream air which facilitates the feeding of nano-oil affects the formation of a protective film [34]. It is believed that the formation of a protective film is from a mixture of chemical reaction film and Al_2O_3 produced in the surface of AL6061-T6 alloy as shown in Fig. 10a and b. These information can be verified by the field emission scanning electron microscopy (FE-SEM) result as shown in Fig. 11.The development of Al_2O_3 is attributable to the natural properties of aluminum alloy, as an oxide layer will always form on its surface. Therefore, at higher atmospheric carrier gas pressure, the oxygen content which may adsorb onto the aluminum surface and hasten the formation of Al_2O_3 will also be elevated [35]. The cause of higher cutting force in machining is the surface Al_2O_3 layer. Higher cutting force may be due to smaller rake angles induced by hard protective film, which would increase the friction at the tool's rake face. Hence, the temperature of some thin layers on the back of the chip adjacent to the tool's rake face could approach

Table 8 Interaction data analysis for cutting force

A×B	B1	B2	B3	B4	Total	Highest total response
A1	−42.21	−40.68	−40.43	−41.95	−165.27	
A2	−42.31	−40.85	−42.90	−40.28	−166.35	
A3	−42.43	−41.23	−41.83	−40.66	−166.15	
A4	−40.28	−40.60	−39.44	−40.07	−160.38	A4
Total	−167.23	−163.36	−164.59	−162.96		
Highest total response				B4		
A×C	C1	C2	C3	C4	Total	Highest total response
A1	−42.21	−40.68	−40.43	−41.95	−165.27	
A2	−40.85	−42.31	−40.28	−42.90	−166.35	
A3	−41.83	−40.66	−42.43	−41.23	−166.15	
A4	−40.07	−39.44	−40.60	−40.28	−160.38	A4
Total	−164.95	−163.09	−163.75	−166.36		
Highest total response		C2				
B×C	C1	C2	C3	C4	Total	Highest total response
B1	−42.21	−42.31	−42.43	−40.28	−167.23	
B2	−40.85	−40.68	−40.60	−41.23	−163.36	
B3	−41.83	−39.44	−40.43	−42.90	−164.59	
B4	−40.07	−40.66	−40.28	−41.95	−162.96	B4
Total	−164.95	−163.09	−163.75	−166.36	−162.96	
Highest total response		C2				

melting point. Associated with the higher temperature, strain energy effects and the presence of extreme pressure additives in cutting oil, chemical reaction films are additionally formed on the machined surface [36]. With this, there is welded form on the protective film. The welded area of Al_2O_3 has a slightly higher hardness profile compared to the pure oxide layer of

Table 9 Interaction data analysis for cutting temperature

A×B	B1	B2	B3	B4	Total	Highest total response
A1	−31.16	−29.85	−32.79	−31.14	−124.94	
A2	−31.44	−30.87	−31.57	−30.60	−124.48	
A3	−30.82	−32.09	−30.81	−29.64	−123.35	A3
A4	−30.72	−34.15	−30.75	−30.68	−126.30	
Total	−124.13	−126.95	−125.92	−122.07		
Highest total response				B4		
A×C	C1	C2	C3	C4	Total	Highest total response
A1	−31.16	−29.85	−32.79	−31.14	−124.94	
A2	−30.87	−31.44	−30.60	−31.57	−124.48	
A3	−30.81	−29.64	−30.82	−32.09	−123.35	A3
A4	−30.68	−30.75	−34.15	−30.72	−126.30	
Total	−123.52	−121.67	−128.36	−125.51		
Highest total response		C2				
B×C	C1	C2	C3	C4	Total	Highest total response
B1	−31.16	−31.44	−30.82	−30.72	−124.13	
B2	−30.87	−29.85	−34.15	−32.09	−126.95	
B3	−30.81	−30.75	−32.79	−31.57	−125.92	
B4	−30.68	−29.64	−30.60	−31.14	−122.07	B4
Total	−123.52	−121.67	−128.36	−125.51		
Highest total response		C2				

Table 10 Interaction data analysis for surface roughness

A×B	B1	B2	B3	B4	Total	Highest total response
A1	−5.61	−11.42	4.81	−0.24	−12.45	
A2	0.28	−1.71	−1.70	0.26	−2.87	
A3	0.39	8.15	−3.38	−1.26	3.91	A3
A4	0.82	0.45	−1.04	1.80	2.03	
Total	−4.12	−4.53	−1.31	0.57		
Highest total response				B4		
A×C	C1	C2	C3	C4	Total	Highest total response
A1	−5.61	−11.42	4.81	−0.24	−12.45	
A2	−1.71	0.28	0.26	−1.70	−2.87	
A3	−3.38	−1.26	0.39	8.15	3.91	A3
A4	1.80	−1.04	0.45	0.82	2.03	
Total	−8.91	−13.43	5.92	7.03		
Highest total response				C4		
B×C	C1	C2	C3	C4	Total	Highest total response
B1	−5.61	0.28	0.39	0.82	−4.12	
B2	−1.71	−11.42	0.45	8.15	−4.53	
B3	−3.38	−1.04	4.81	−1.70	−1.31	
B4	1.80	−1.26	0.26	−0.24	0.57	B4
Total	−8.91	−13.43	5.92	7.03		
Highest total response				C4		

aluminum alloy [37]. Therefore, to overcome the hardness of the welded form on the protective film, elevated cutting force is necessary. However, the surface roughness results shown in Table 6 illustrate that surface roughness first decreases and then extremely increases when air pressure is beyond 2 bars. This may be due to the reason given above, of higher air pressure leading to the formation of a welded area. Such weld could act as a peeler that may mechanically pull away some workpiece material [38]. When a rise in air pressure occurs, it helps accelerate the nano-oil into the deep cutting zone and assists with polishing the machined surface.

At the same time, nozzle orientation is a key factor in high speed machining. The variations of cutting oil feed orientation are shown in Fig. 1. The best cutting temperature is displayed at a 30° nozzle angle, where heat successfully gets drawn from the surface of the workpiece. However, at 30° nozzle angle the highest surface roughness and chip thickness ratio are witnessed. This phenomenon may be related to the fact that this orientation is not suitable for accelerating the cutting oil into the cutting region and does not assist machining toward achieving enhanced surface quality. As previously mentioned, the cutting oil in the tool–chip interface has negligible effect on the cutting force and stress in the cutting edge. Therefore, a 30° nozzle angle may be optimal for cutting force.

The particles may get partially embedded into the machined surface when it collides with the asperities during the process of polishing, and due to extremely high pressure in the cutting zone the particles may split and change form upon

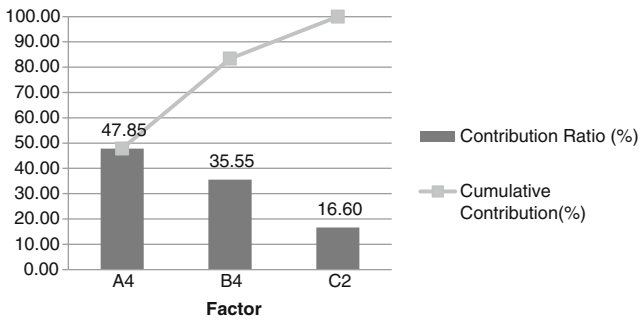

Fig. 7 The diagram of contribution and cumulative contribution for cutting force

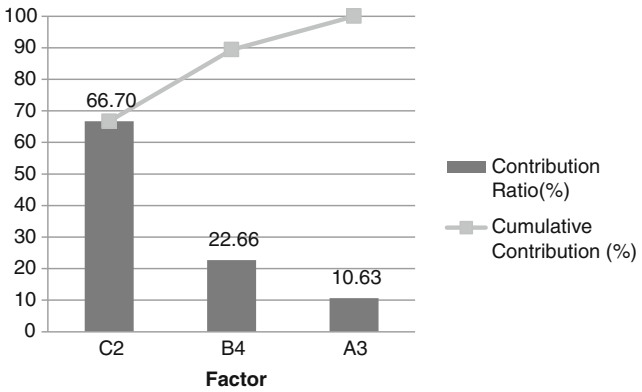

Fig. 8 The diagram of contribution and cumulative of contribution for cutting temperature

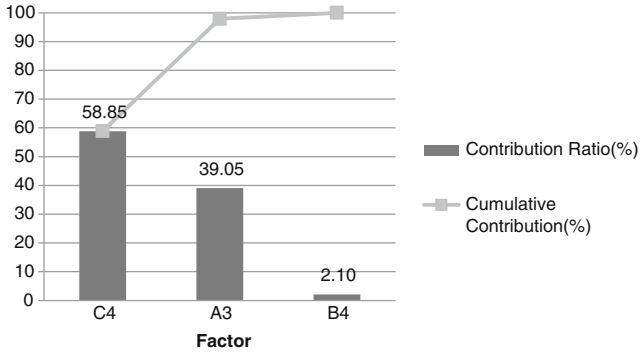

Fig. 9 The diagram of contribution and cumulative contribution for surface roughness

being flattened. The shear-off debris could continue to support cutting, but not as well as spherical nanoparticles that can exercise rolling behavior with a low coefficient of friction. At higher concentrations of nanoparticles, the partially embedded particles might plough off new nanoparticles, and both will then continue to polish the surface. The ploughed off particles will leave thin exfoliated film on the contact spot due to damage from high loading [39]. Meanwhile, when nanoparticle concentration keeps increasing, those nanoparticles may infuse into the surface pores and get trimmed by other oncoming nanoparticles. The reason for this is that perhaps the rolling of nanoparticles leads to the formation of an easy-to-shear lubrication film [40] as well as surface severities, polishing the surface and enhancing quality. Consequently, the impact of MoS_2 particles encountered on intermetallic particles might increase cutting force. For these reasons, inappropriately feeding nano-oil may negatively impact the cutting operation.

4.1 Confirmation test

The latest stage in the Taguchi optimization method is to conduct a confirmation test with the following optimal parameter combinations: A4 B4 C2 for cutting force, A3 B4 C2 for cutting temperature and A3 B4 C4 for surface roughness. The aim is to confirm the recommendation after the finest levels of all control factors. Measurements were taken three times and the averages of the measured cutting forces, cutting temperature and surface roughness were calculated as shown in Table 11. The outcome demonstrates improvements of 2.62 %, 0.04 % and 2.56 % for cutting force, cutting temperature and surface roughness, respectively, compared to the lowest values obtained from the experiments shown in Table 6.

5 Conclusions

In this investigation, the optimal MoS_2 nanolubrication parameters in milling aerospace Al6061-T6 alloy were explored with the aim of increasing machining performance. The slot-milling experiment was done as a case study on the cutting process of a rectangular workpiece of Aluminum AL6061-T6 alloy, which is a material commonly used in the aerospace industries. The nanoparticle oil was prepared by adding MoS_2 nanoparticles of roughly 20–60 nm to the mineral oil in the

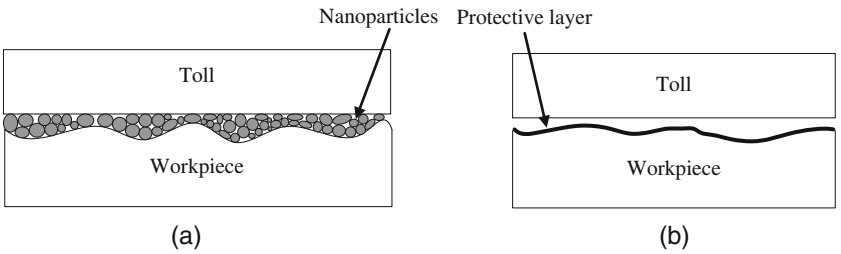

Fig. 10 The presence of rolling effect (**a**) and protective film (**b**) on the machined surface

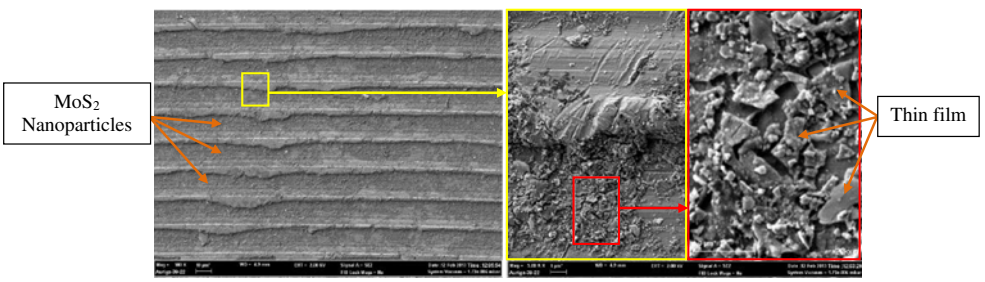

Fig. 11 FE-SEM on a sample which machined with 0.5 wt.% concentration of MoS_2

Table 11 Confirmation test

Confirmation test no.	Control factors and levels (i)			Measured values										
	Nanoparticle suspended concentration (A)	Air pressure (B)	Nozzle orientation (C)	Cutting force (N)				Cutting temperature (°C)				Surface roughness, R_a (μm)			
				Reading			Average	Reading			Average	Reading			Average
				1	2	3		1	2	3		1	2	3	
1	$i=4$	4	2	91.34	91.03	91.18	91.18	33.30	34.20	33.10	33.53	0.79	0.72	0.71	0.74
2	$i=3$	4	2	113.95	102.37	111.85	109.39	33.30	30.40	29.90	30.20	1.19	1.20	1.24	1.21
3	$i=3$	4	2	138.91	117.35	139.36	131.87	30.20	31.60	31.40	31.07	0.37	0.36	0.41	0.38

ultra-sonic mixture for 48 h in order to suspend the particles homogeneously. To distribute the oil to the tool–chip interface area, the MQL equipment with a thin-pulsed jet nozzle was employed. With respect to the nanolubrication system, the nozzle was equipped with an additional air nozzle to increase the speed of the lubricant entering the cutting region. From the Taguchi optimization method and based on the results achieved, the following deductions can be made:

1. Cutting force can be minimized by applying 1 wt.% nanoparticle suspended concentration in the mineral oil, high air stream pressure (4 bars) and 30° nozzle orientation angle.
2. The minimum cutting temperature is achieved with 0.5 wt.% nanoparticle concentration in the mineral oil, higher air stream pressure (4 bars) and 30° nozzle orientation angle.
3. The best surface roughness can be achieved with a nanoparticle concentration of 0.5 wt.% in oil, higher air pressure (4 bars) and higher nozzle orientation angle (60°).

The presentation above of unmodified oil and the extreme decrease of cutting oil consumption leads to the conclusion that minimal quantity lubrication oil mixed with a nanoparticle additive is practical for enhancing the machining process. With the low cost, outstanding properties of MoS_2 nanoparticles, and environmental benefit, they might make for a new and effective alternative to flood lubrication.

Acknowledgment The authors acknowledge the financial support under the University Malaya Research Grant (Grant No.: UM.TNC2/RC/AET/GERAN (UMRG) RG128/11AET) from the University of Malaya, Malaysia.

Reference

1. Lakshminarayanan A, Balasubramanian V, Elangovan K (2009) Effect of welding processes on tensile properties of AA6061 aluminium alloy joints. Int J Adv Manuf Technol 40:286–296
2. Shankar MR, Chandrasekar S, Compton WD, King AH (2005) Characteristics of aluminum 6061-T6 deformed to large plastic strains by machining. Mater Sci Eng A 410–411:364–368
3. Li Y, Liang SY (1999) Cutting force analysis in transient state milling processes. Int J Adv Manuf Technol 15:785–790
4. Hsu SM (2004) Nano-lubrication: concept and design. Tribol Int 37: 537–545
5. Lee J, Cho S, Hwang Y, Cho HJ, Lee C, Choi Y, Ku BC, Lee H, Lee B, Kim D, Kim SH (2009) Application of fullerene-added nano-oil for lubrication enhancement in friction surfaces. Tribol Int 42:440–447
6. Tao X, Jiazheng Z, Kang X (1996) The ball-bearing effect of diamond nanoparticles as an oil additive. J Phys D Appl Phys 29:2932–2937
7. Lathkar GS, Bas USK (2000) Clean metal cutting process using solid lubricants. In: Proceedings of the 19th AIMTDR conference. Narosa Publishing House IIT Madras, pp 15–31

8. Reddy NSK, Nouari M, Yang M (2010) Development of electrostatic solid lubrication system for improvement in machining process performance. Int J Mach Tools Manuf 50:789–797
9. Dilbag S, Rao PV (2008) Performance improvement of hard turning with solid lubricants. Int J Adv Manuf Technol 38: 529–535
10. Sharma VS, Dogra M, Suri NM (2009) Cooling techniques for improved productivity in turning. Int J Mach Tools Manuf 49:435–453
11. Sreejith PS, Ngoi BKA (2000) Dry machining: machining of the future. J Mater Process Technol 101:287–291
12. Klocke F, Eisenblätter G (1997) Dry cutting. CIRP Ann Manuf Technol 46:519–526
13. Lee P, Naam JS, Li C, Lee SW (2012) An experimental study on micro-grinding process with nanofluid minimum quantity lubrication (MQL). Int J Precis Eng Manuf 13(3):331–338
14. He S (1982) Solid lubrication materials for high temperature: a review. Tribol Int 15:303–314
15. Miaosun S (2000) Solid lubrication materials. China Chemistry Press, Beijing
16. Nakamura T, Tanaka S, Hayakawa K, Fukai Y (2000) A study of the lubrication behavior of solid lubricants in the upsetting process. J Tribol 122:803–808
17. Alberts M, Kalaitzidou K, Melkote S (2009) An investigation of graphite nanoplatelets as lubricant in grinding. Int J Mach Tools Manuf 49:966–970
18. Deshmukh SD, Basu SK (2006) Significance of solid lubricants in metal cutting, in: 22nd AIMTDR
19. Sayuti M, Sarhan AAD, Hamdi M (2013) An investigation of optimum SiO_2 nanolubrication parameters in end milling of aerospace Al6061-T6 alloy. Int J Adv Manuf Technol 67(1–4): 833–849
20. Keblinski P, Phillpot SR, Choi SUS, Eastman JA (2002) Mechanisms of heat flow in suspensions of nano-sized particles (nanofluids). Int J Heat Mass Transf 45:855–863
21. Wang W, Liu K, Jiao M (2007) Thermal and non-Newtonian analysis on mixed liquid–solid lubrication. Tribol Int 40:1067–1074
22. Lee JH, Hwang KS, Jang SP, Lee BH, Kim JH, Choi SUS, Choi CJ (2008) Effective viscosities and thermal conductivities of aqueous nanofluids containing low volume concentrations of Al_2O_3 nanoparticles. Int J Heat Mass Transf 51:2651–2656
23. Murshed SMS, Leong KC, Yang C (2009) A combined model for the effective thermal conductivity of nanofluids. Appl Therm Eng 29: 2477–2483
24. Masmiati N, Sarhan AAD, Hamdi M (2012) Optimizing the cutting parameters for better surface quality in 2.5D cutting utilizing titanium coated carbide ball end mill. Int J Precis Eng Manuf 13(12):2097–2102
25. Davis JR (1990) Metals handbook, Vol. 2 — Properties and selection: Nonferrous alloys and special-purpose material, 10th edn. ASM International, Materials Park, OH
26. Liew WYH (2010) Low-speed milling of stainless steel with TiAlN single-layer and TiAlN/AlCrN nano-multilayer coated carbide tools under different lubrication conditions. Wear 269:617–63
27. Yan J, Zhang Z, Kriyagawa T (2011) Effect of nano-particle lubrication in diamond turning of reaction-bonded SiC. Int J Autom Technol 5:307–312
28. Hung TC, Su YT (2006) A method for reducing tool wear in a polishing process. Int J Mach Tools Manuf 46:413–423
29. Wu YY, Tsui WC, Liu TC (2007) Experimental analysis of tribological properties of lubricating oils with nanoparticle additives. Wear 262:819–825
30. Mu-Jung Kao CRL (2009) Evaluating the role of spherical titanium oxide nanoparticles in reducing friction between two pieced of cast iron. J Alloys Compd 483:456–459
31. Sarhan AAD, Sayuti M, Hamdi M (2012) Reduction of power and lubricant oil consumption in milling process using a new SiO_2 nanolubrication system. Int J Adv Manuf Technol 63(5–8):505–512
32. Yousefi YIR (2000) A study on ultra-high-speed cutting of aluminium alloy: formation of welded metal on the secondary cutting edge of the tool and its effects on the quality of finished surface. J Int Soc Precis Eng Nanotechnol 24:371–376
33. N Suresh Kumar Reddy, P Venkateswara Rao (2006) Experimental investigation to study the effect of solid lubricants on cutting forces and surface quality in end milling. Int J Mach Tools Manuf 46:189–198
34. Sayuti M, Sarhan AAD, Tanaka T, Hamdi M, Saito Y (2013) Cutting force reduction and surface quality improvement in machining of aerospace duralumin AL-2017-T4 using carbon onion nanolubrication system. Int J Adv Manuf Technol 65(9–12):1493–1500
35. Wakabayashi SST, Inasaki I, Terasaka K, Musha Y, Toda Y (2007) Tribological action and cutting performance of MQL media in machining of aluminium. Ann CIRP 56/1
36. Lin HSYC (2004) Limitations on use of ZDDP as an antiwear additive in boundary lubrication. Tribol Int 37:25–33
37. Prado LEMRA, Shindo DJ, Soto KF (2001) Tool wear in the friction-stir welding of aluminium alloy 6061 + 20% Al_2O_3: a preliminary study. Scr Mater 45:75–80
38. Hamdan AA, Sarhan AAD, Hamdi M (2012) An optimization method of the machining parameters in high speed machining of stainless steel using coated carbide tool for best surface finish. Int J Adv Manuf Technol 58(1):81–91
39. Rapoport ONL, Lapsker I, Verdyan A, Moshkovich A, Feldman Y, Tenne R (2005) Behavior of fullerene-like WS2 nanoparticles under severe contact conditions. Wear 259:703–707
40. Rapoport VLL, Lvovsky M, Nepomnyashchy O, Volovik Y, Tenne R (2002) Mechanism of friction of fullerenes. Ind Lubr Tribol 54:171–176